Highly Electrochemical Reaction of Lithium in the Ordered Mesoporosus β-MnO_2

Jia-Yan Luo, Jing-Jun Zhang, and Yong-Yao Xia*

Chemistry Department and Shanghai Key Laboratory of Molecular Catalysis and Innovative Materials, Fudan University, Shanghai 200433, People's Republic of China

Received June 23, 2006. Revised Manuscript Received August 15, 2006

The highly crystallized β-MnO_2 with the narrowest [1 × 1] channels prepared by direct thermal decomposition of $Mn(NO_3)_2$ does not provide much capacity due to the poor kinetics of the lithium intercalation/deintercalation process. In the present work, we report the preparation and electrochemical performance of an ordered mesoporous β-MnO_2 as a positive electrode for rechargeable lithium batteries. The well-ordered mesoporous β-MnO_2 prepared using mesoporous silica KIT-6 as a template by thermal decomposition of $Mn(NO_3)_2$ exhibits high initial capacity, reaching a chemical composition of $Li_{0.75}$-MnO_2, and it also shows a good rate capability and cycling ability. The correlation between the specific mesoporous structure and the superior electrochemical performance was discussed in detail.

Introduction

Manganese dioxides exists in many forms, for example, the hollandite structured α-MnO_2 with [2 × 2] and [1 × 1] channels, rutile structured β-MnO_2 with the narrowest [1 × 1] channels, γ-MnO_2 containing domains of intergrown β-MnO_2, ramsdellite MnO_2 with large [1 × 2] channels, and spinel structured λ-MnO_2 with a three-dimensional network of channels. Most of manganese dioxides, α-MnO_2, γ-MnO_2, and λ-MnO_2, can accommodate significant lithium in the structure, giving a large capacity as a cathode material for lithium batteries.[1−7] However, β-MnO_2 with the narrowest [1 × 1] channels among the channel-type manganese family does not provide much capacity due to the poor kinetics of the lithium intercalation/deintercalation process when highly crystalline products prepared by direct thermal decomposition of $Mn(NO_3)_2$ are employed. It has been reported that the amount of electrochemical reaction of lithium into the crystallized β-MnO_2 was less than $Li_{0.3}MnO_2$ at room temperature, and it reaches near $Li_{0.75}MnO_2$ only in the poorly crystallized products prepared from λ-MnO_2 and the β-MnO_2/acetylene black (AB) composite; however, the capacity fades quickly due to a transformation of β-MnO_2 to the $LiMn_2O_4$ spinel structure.[8−13]

The morphology and surface area of particles within an electrode have a profound effect on the electrochemical properties of a material. By creating electrode materials with unique nanostructure, the electrochemical performance of many materials has been markedly improved.[14−18] In recent years, with the rapid development of mesoporous nanostructure, the synthesis of electrode materials with mesoporous nanostructure has attracted intensive attention and shown great promise for boosting the performance of rechargeable lithium-ion batteries. It has been found that the resulting energy density, cycle life, and rate performance of rechargeable lithium-ion batteries are dramatically improved by the unique mesoporous nanostructure of the active materials in the electrode,[19−26] since the larger specific surface area of these materials leads to higher current density and the thin

* Corresponding author. Fax: (+86) 21-5566-4177. E-mail: yyxia@fudan.edu.cn.

(1) Thackeray, M. M.; Rossouw, M. H.; Kock, A.; Harpe, A. P. *J. Power Sources* **1993**, *43*−*44*, 289.
(2) Thackeray, M. M. *Mater. Res. Bull.* **1983**, *18*, 461.
(3) Gummow, R. J.; Kock, A.; Thackeray, M. M. *Solid State Ionics* **1994**, *69*, 59.
(4) Tarascon, J. M.; Guyomard, D. *Electrochim. Acta* **1993**, *38*, 1221.
(5) Xu, J. J.; Jain, G.; Yang, J. S. *Electrochem. Solid-State Lett.* **1993**, *5*, A152.
(6) Zhu, S. M.; Zhou, H. S.; Hibino, M.; Honma, I.; Ichihara, M. *Adv. Funct. Mater.* **2005**, *15*, 381.
(7) Armstrong, A. R.; Bruce, P. G. *Nature* **1996**, *381*, 499.
(8) Murphy, D. W.; Salvo, F. J. Di; Carides, J. N.; Waszczak, J. V. *Mater. Res. Bull.* **1978**, *13*, 1395.
(9) Thackeray, M. M.; Kock, A.; Picciotto, L. A. *J. Power Sources* **1989**, *26*, 355.
(10) David, W. I. F.; Thackeray, M. M.; Bruce, P. G.; Goodenough, J. B. *Mater. Res. Bull.* **1984**, *19*, 99.
(11) Zachau-Christiansen, B.; West, K.; Jacobsen, T.; Skaarup, S. *Solid State Ionics* **1984**, *70*−*71*, 401.
(12) Cheng, F. Y.; Zhao, J. Z.; Song, W. N.; Li, C. S.; Ma, H.; Chen, J.; Shen, P. W. *Inorg. Chem.* **2006**, *45*, 2038.
(13) Tang, W. P.; Yang, X. J.; Liu, Z. H.; Ooi, K. *J. Mater. Chem.* **2003**, *13*, 2989.
(14) Li, H.; Shi, L. H.; Lu, W.; Huang, X. J.; Chen, L. Q. *J. Electrochem. Soc.* **2001**, *148*, A915.
(15) Li, H.; Wu, X.; Chen, L. Q.; Huang, X. J. *Solid State Ionics* **2003**, *149*, 185.
(16) Zhang, S. S.; Ding, M. S.; Xu, K.; Allen, J.; Jow, T. R. *Electrochem. Solid-State Lett.* **2001**, *4*, A206.
(17) Li, H.; Shi, L. H.; Wang, Q.; Chen, L. Q.; Huang, X. J. *Solid State Ionics* **2002**, *148*, 247.
(18) Doi, T.; Iriyama, Y.; Abe, T.; Ogumi, Z. *Chem. Mater.* **2005**, *17*, 1580.
(19) Zhou, H. S.; Zhu, S. M.; Hibino, M.; Honma, I.; Ichihara, M. *Adv. Mater.* **2003**, *15*, 2107.
(20) Zhu, S. M.; Zhou, H. S.; Miyoshi, T.; Hibino, M.; Honma, I.; Ichihara, M. *Adv. Mater.* **2004**, *16*, 2012.
(21) Kim, E.; Son, D.; Kim, T. C.; Cho, J.; Park, B.; Ryu, K. S.; Chang, S. H. *Angew. Chem., Int. Ed.* **2004**, *43*, 5987.
(22) Liu, P.; Lee, S. H.; Tracy, C. E.; Yan, Y. F.; Turner, J. A. *Adv. Mater.* **2002**, *14*, 27.
(23) Zhou, H. S.; Lin, D. L.; Hibino, M.; Honma, I. *Angew. Chem., Int. Ed.* **2005**, *44*, 797.
(24) Zhou, H. S.; Lin, D. L.; Honma, I. *Nat. Mater.* **2004**, *3*, 65.
(25) Wang, H. Y.; Abe, T.; Maruyama, S.; Iriyama, Y.; Ogumi, Z.; Yoshikawa, K. *Adv. Mater.* **2005**, *17*, 2857.

10.1021/cm061458o CCC: $33.50
Published on Web 10/14/2006

pore wall can reduce the lithium ion diffusion path. In addition, the mesoporous structure facilitates the fast transport of electrolyte with lithium ion and can also act as a buffer layer to alleviate the volume expansion of the electrode materials during lithiation/delithiation.

Non-siliceous mesoporous materials, especially transition-metal oxides, can be prepared using a so-called soft templating method in a similar way to synthesize ordered mesoporous silica. However, direct synthesis of these kinds of mesoporous materials is quite difficult because, compared to silica, the surfactant/oxide composition precursors are often susceptible to lack of condensation, redox reactions, or phase transitions accompanied by the thermal breakdown of the structural integrity.[27−31] Another method, using the hard templates to nanocast non-siliceous materials, has also been developed in the recent years.[31−34] Bruce's group has recently been successful in using the three-dimensional caged mesoporous silica, KIT-6, to synthesize ordered mesoporous metal oxides and even alkali metals containing oxides.[35−37] Herein, we for the first time report the synthesis of a highly ordered mesoporous β-MnO_2 and test its electrochemical performance as a cathode material for lithium batteries by means of cyclic voltammetry and a galvanostatic method and compared the results with those of conventional β-MnO_2 by directly calcining $Mn(NO_3)_2 \cdot 4H_2O$ at 350 °C. The results demonstrate that the β-MnO_2 with mesoporous nanostructure exhibits high initial capacity, giving rise to a composition of $Li_{0.75}MnO_2$, and a good rate discharge performance and cycling life, indicating that β-MnO_2 with mesoporous nanostructure is a promising cathode active material for advanced rechargeable lithium batteries.

Experimental Section

Sample Preparation and Characterization. The β-MnO_2 with regular mesoporosity was synthesized using mesoporous silica KIT-6 as a template. Mesoporous silica KIT-6 was prepared according to the reported procedure.[38,39] In a typical synthesis, 6 g of $Mn(NO_3)_2 \cdot 4H_2O$ (50%) was dissolved in 25 mL of ethanol, and then 1 g of KIT-6 was added to the above solution. The mixture was stirred overnight, and then a powder specimen was obtained; the solid was then calcined in a muffle furnace with a heating rate of 1 °C/min from room temperature to 350 °C and then maintained at 350 °C for 5 h. The β-MnO_2 with ordered mesoporous structure was obtained through the solution etching of silica framework by a 2 M NaOH solution. Centrifugation was preferred to separate the final products, and washing with distilled water and ethanol was also performed. The conventional β-MnO_2 was prepared by directly calcining $Mn(NO_3)_2 \cdot H_2O$ at 350 °C for 5 h. Small-angle and wide-angle XRD measurements were performed on a Rigaku D/MAX-IIA X-ray diffractometer using Cu Kα radiation. SEM images were obtained on Philip XL30. TEM was performed using a JEOL JEM-2010 electron microscope. Nitrogen adsorption−desorption measurements were performed on a Micromeritics Tristar 3000 system at 77 K.

Electrochemical Measurements. The charge/discharge test was characterized in a CR2032-type coin cell. Metallic lithium was used as the negative electrode. The working electrode was fabricated by compressing a mixture of the active materials (mesoporous β-MnO_2 or conventional β-MnO_2), conductive material (AB), and binder (poly(tetrafluoroethylene) (PTFE)) in a weight ratio of β-MnO_2/AB/PTFE = 16:3:1 onto an aluminum grid at 10 MPa. The electrodes were punched in the form of disks typically with a diameter of 12 mm. The typical mass load of the active material is about 10 mg/cm^2. The electrode was dried at 120 °C for 12 h before assembly. The cell assembly was operated in a glovebox filled with pure argon. The electrolyte solution was 1 M $LiPF_6$/ethylene carbonate (EC)/dimethyl carbonate/ethyl methyl carbonate (1:1:1 by volume). Lithium insertion into MnO_2 electrode was referred to as discharge, and extraction was referred to as charge. The cell capacity was determined by only the positive active material. Cyclic voltammograms (CVs) were characterized using a three-electrode cell; the metallic lithium was used as the counter and reference electrodes. The experiments were performed using a Solartron Instrument model 1287 electrochemical interface controlled by a computer at a scanning rate of 0.1 mV/s.

Results and Discussion

Following the synthesis procedure given in the experimental section, a mesoscopically ordered array of β-MnO_2 was obtained. Figure 1A shows the small-angle X-ray diffraction (XRD) pattern of the β-MnO_2. The characteristic diffraction peaks of the Ia 3d cubic structure of the mesoporous β-MnO_2 can be observed although the higher-order reflections are not very pronounced or well-resolved. The wide-angle XRD patterns of the as-synthesized mesoporous and conventional β-MnO_2 are shown in Figure 1B. It can be observed that there is no distinct difference in peak position of the two products, whereas the peak intensity rather differs from one to the other. A little broadening of the peaks for the mesoporous sample is owed to the very fine grain size and defect along the channel produced in the decomposition process. Both the diffraction peaks of the two products can be readily indexed to the pure tetragonal phase of β-MnO_2 [space group $P4_2/mnm$]. No peaks from other phases have been detected, indicating that the products are of high purity. According to Scherrer's method, one deduces a crystallite dimension of about 25.5 nm along the [110] direction and 19.5 nm along the [002] direction for the conventional β-MnO_2, while about 6.2 nm along the [110] direction and 13.5 nm along the [002] direction for the mesoporous β-MnO_2 are deduced, suggesting that the mesoporous β-MnO_2 tends to be oriented along the *c*-axis.

Figure 2 compares the scanning electron microscopy (SEM) images of the mesoporous β-MnO_2 and conventional

(26) Yoshio, M.; Wang, H. Y.; Fukuda, K. *Angew. Chem., Int. Ed*. **2003**, *42*, 4203.
(27) Schüth, F. *Chem. Mater*. **2001**, *13*, 3184.
(28) Soler-Illia, G.; Sanchez, C.; Lebeau, B.; Patarin, J. *Chem. Rev*. **2002**, *102*, 4093.
(29) Malik, A. S.; Duncan, M. J.; Bruce, P. G. *J. Mater. Chem.* **2003**, *9*, 2123.
(30) Jiao, F.; Bruce, P. G. *Angew. Chem., Int. Ed*. **2004**, *43*, 5958.
(31) Wang, Y. Q.; Yang, C. M.; Schmidt, W.; Spliethoff, B.; Bill, E.; Schüth, F. *Adv. Mater*. **2005**, *17*, 53.
(32) Ryoo, R.; Joo, S. H.; Jun, S. *J. Phys. Chem. B* **1999**, *103*, 7743.
(33) Tian, B. Z.; Liu, X. Y.; Yang, H. F.; Xie, S. H.; Yu, C. Z.; Tu, B.; Zhao, D. Y. *Adv. Mater*. **2003**, *15*, 1370.
(34) Jiao, F.; Yue, B. Zhu. K. K.; Zhao, D. Y.; He, H. Y. *Chem. Lett.* **2003**, *32*, 770.
(35) Bruce, P. G. *Solid State Sci.* **2005**, *7*, 1456.
(36) Jiao, F.; Harrison, A.; Jumas, J. C.; Chadwick, A. V.; Kockelmann, W.; Bruce, P. G. *J. Am. Chem. Soc*. **2006**, *128*, 5468.
(37) Jiao, F.; Shaju, K. M.; Bruce, P. G. *Angew. Chem., Int. Ed*. **2005**, *44*, 6050.
(38) Kleitz, F.; Choi, S. H.; Ryoo, R. *Chem. Commun.* **2003**, *17*, 2136.
(39) Kim, T. W.; Kleitz, F.; Paul, B.; Ryoo, R. *J. Am. Chem. Soc*. **2005,** *127*, 7601.

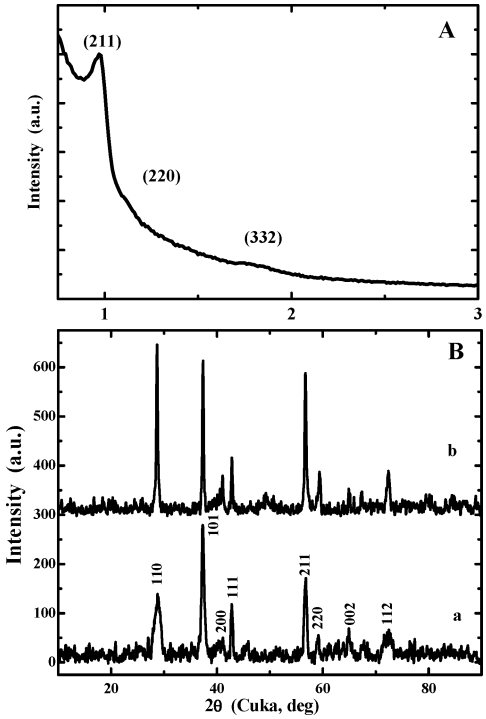

Figure 1. (A) Low-angle XRD pattern of mesoporous β-MnO_2, and (B) wide-angle XRD patterns of (a) mesoporous and (b) conventional β-MnO_2.

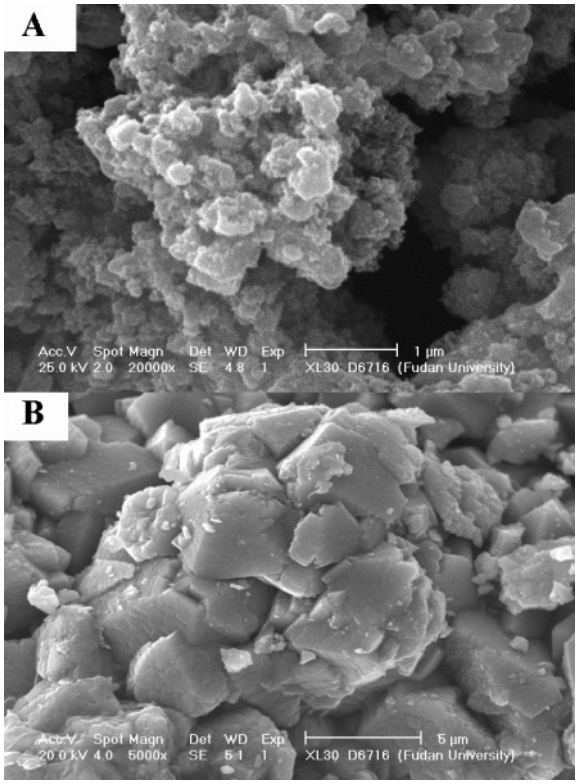

Figure 2. SEM images of (A) mesoporous β-MnO_2 and (B) conventional β-MnO_2.

β-MnO_2; both MnO_2 consist of agglomerated small grains. The mesoporous β-MnO_2 has a rough surface and smaller particle, while the conventional β-MnO_2 has a larger taping particle and very smooth surface.

The replication of the KIT-6 silica by MnO_2 can also be directly observed in the transmission electron microscopy (TEM) images taken along different axes. The hexagonal image contrast pattern in Figure 3A, where the mesoporous

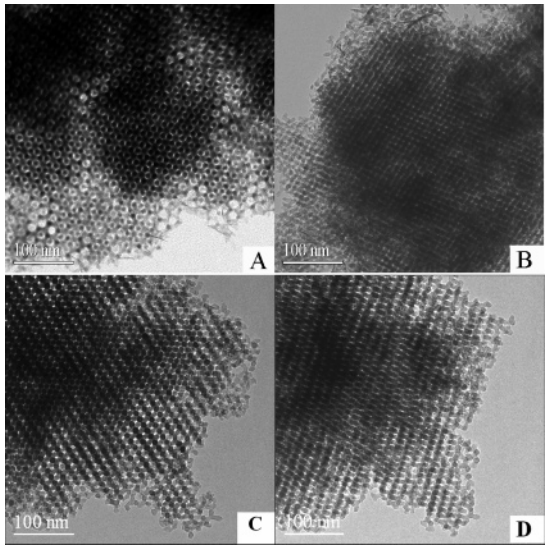

Figure 3. TEM images of mesoporous β-MnO_2 viewed down the (A) [111], (B) [531], (C) [210], and (D) [311] zone axis.

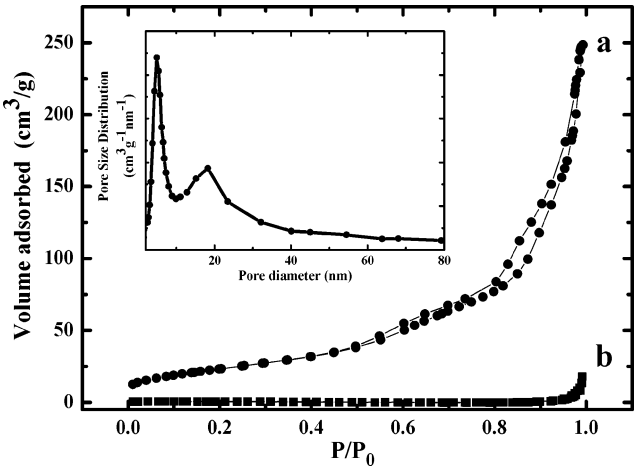

Figure 4. Nitrogen adsorption−desorption isotherms at 77 K of (a) mesoporous β-MnO_2 and (b) conventional β-MnO_2. The inset is the pore size distribution of mesoporous β-MnO_2.

channels are seen as bright contrast, indicates that the image is viewed down the [111] zone axis of the KIT-6 related cubic unit cell and the cell dimension is similar to that of KIT-6, which is in good agreement with the small-angle XRD in Figure 1A. Figure 3B−D are other TEM images of mesoporous β-MnO_2 viewed down the [531], [210], and [311] zone axes of the KIT-6 related cubic mesostructural unit cell, respectively. Figure 4 shows the nitrogen adsorption−desorption isotherms of mesoporous and conventional β-MnO_2. The isotherms mesoporous β-MnO_2 are of typical IV classification with a clear H_1-type hysteretic loop, which is characteristic of mesoporous materials. The mesoporous β-MnO_2 sample has a surface area of 84 $m^2\ g^{-1}$ and a pore volume of 0.38 $cm^3\ g^{-1}$, which are much larger than those of conventional β-MnO_2 with a surface area of 0.6 $m^2\ g^{-1}$ and a pore volume of 0.01 $cm^3\ g^{-1}$. The pore size distribution of mesoporous β-MnO_2 centers at 4.9 and 18.2 nm, while the former reflects the minimum wall thickness of KIT-6 whereas the latter is corresponding to the wall junctions in KIT-6 or to the pores between the particles.

Cyclic voltammetry was used to investigate the electrochemical behavior of the highly ordered mesoporous β-MnO_2.

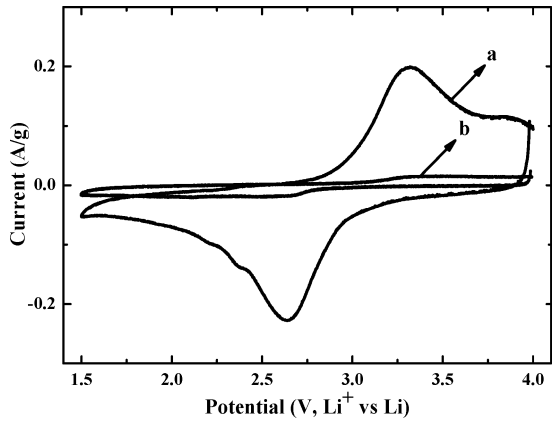

Figure 5. CVs of (a) mesoporous β-MnO_2 and (b) conventional β-MnO_2 at a scan rate of 0.1 mV s^{-1}.

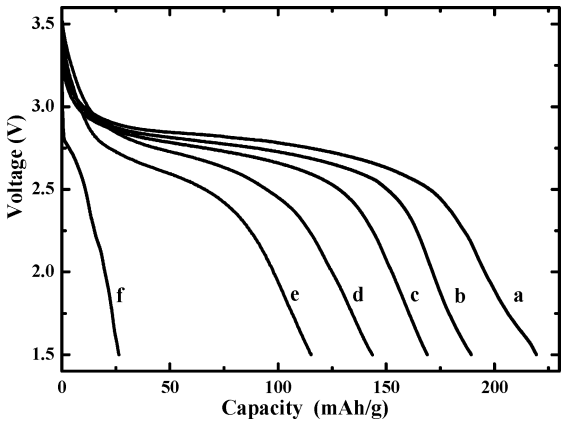

Figure 6. First discharge curves of (a) mesoporous β-MnO_2 at a current rate of 0.03 mA/cm^2, (b) mesoporous β-MnO_2 at a current rate of 0.1 mA/cm^2, (c) mesoporous β-MnO_2 at a current rate of 0. 3 mA/cm^2, (d) mesoporous β-MnO_2 at a current rate of 1 mA/cm^2, (e) mesoporous β-MnO_2 at a current rate of 2 mA/cm^2, and (f) a conventional sample at a current rate of 0.03 mA/cm^2.

Figure 5 compared the CVs of the mesoporous and conventional β-MnO_2 at a scan rate of 0.1 mV s^{-1}. The trace A shows the synthesized ordered mesoporous β-MnO_2 while the trace B shows the conventional sample produced by direct decomposition. A pair of redox peaks at 2.6 and 3.2 V versus Li^+/Li was detected on the mesoporous β-MnO_2, while it was not observed on the conventional MnO_2. The reaction corresponding the redox peak can be expressed by the equation

$$x\mathrm{Li}^+ + \mathrm{MnO_2} + x\mathrm{e}^- \leftrightarrow \mathrm{Li}_x\mathrm{MnO_2}$$

The galvanostatic first discharge behaviors of mesoporous and conventional β-MnO_2 at a constant current density of 0.03 mA/cm^2 are shown in Figure 6. The first discharge curve of mesoporous β-MnO_2 shows a flat plateau in the voltage range between 2.9 and 2.6 V, and the discharge capacity reaches 219 mA h g^{-1} to an end voltage of 1.5 V. This value is several times larger than that in the reported data of β-MnO_2 with one-dimensional nanostructures[9] and even higher than that of the related poor crystalline materials.[12] As for conventional β-MnO_2, the first discharge capacity is less than 30 mA h g^{-1}, which is consistent with earlier reports[8,9] that highly crystalline products prepared by direct thermal decomposition of $Mn(NO_3)_2$ do not provide much capacity during the lithiation/delithiation.

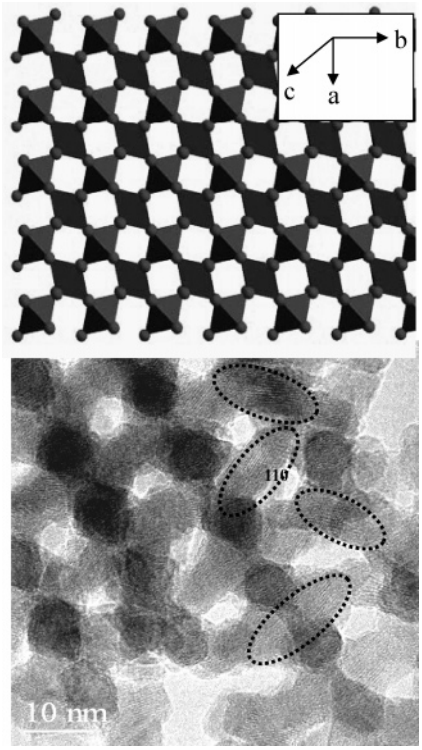

Figure 7. Structure of β-MnO_2 with [1 × 1] channels down the *c*-axis (top) and high-resolution TEM image viewed from the [210] direction (Bottom).

The β-MnO_2 has a rutile-type structure with tetragonal symmetry as shown in Figure 7A. The oxygen ions form a distorted hexagonal-close-packing array. Single strands of edge-sharing MnO_6 octahedra propagate in a direction parallel to the crystallographic ***c***-axis. Due to this special arrangement, Li^+ diffusion in the rutile-type structure is highly anisotropic. As for the conventional β-MnO_2, although the crystallite dimension is relative small, there is no pore between the crystallites for electrolyte to transport ions, as shown in the SEM images and BET analyzed above. Therefore, the lithiation/delithiation probably proceeds only on the surface of secondary particles about 5 um in size, and not much capacity is thus expected. But for the mesoporous β-MnO_2, as demonstrated in the a high-resolution TEM image in Figure 7B, there exists a 4−5 nm mesoporous void between the pore walls, and the pore wall thickness was only 6−7 nm. Assuming that the Li^+ diffusion coefficient in the β-MnO_2 has the same order of that in the same structure rutile TiO_2 ($D \approx 10^{-10}$ m^2/s),[40−42] the rapid Li^+ diffusion along the *c*-axis would suffice for a homogenization of a microcrystalline grain if all the *c*-axis channels are available from the surface (mean square displacement for $t = 1$ s is ca. 10 μm). Therefore, the kinetics-determining process is the primary interfacial Li^+ transfer at the mesoporous wall surface. The uniform mesopores can be easily accessed by an electrolyte containing Li^+ and the large organic solvent molecules of EC and diethyl carbonate. It thus provides an insertion and extraction space inside

(40) Koudriachova, M. V.; Harrison, N. M.; Leeuw, S. W. *Phys. Rev. Lett.* **2001**, *86*, 1275.
(41) Hu, Y. S.; Kienle, L.; Guo, Y. G.; Maier, J. *Adv. Mater.* **2006**, *18*, 14217.
(42) Stashans, A.; Lunell, S.; Bergstroem, R. *Phys. Rev. B* **1996**, *53*, 159.

β-MnO_2 along the inner surface of the mesoporous, which decreases the effective diffusion path and increases the effective surface area for insertion/extraction of Li^+. The result in Figure 7B also shows clearly that the pore wall consists of a microcrystalline grain oriented preferably along the *c*-axis with 6 nm along the [110] direction and 12 nm along the [002] direction. The result is well-consistent with that by XRD analysis. As shown in Figure 7B, the [1 × 1] channel direction in some particles coincides with the mesoporous direction, the (110) plane facing the pore, which is less beneficial for the lithium insertion, but the mesoporous β-MnO_2 surface is also dominated by the (002) faces in which the lithium ion can easily intercalate along the *c*-axis channels. This is also the reason why the mesoporous β-MnO_2 cannot yet deliver the theoretical capacity of 308 mA h g^{-1} even if it shows a higher capacity than that of the highly crystallized β-MnO_2.

Figure 6 also shows the discharge profiles for the first discharge from the open circuit voltage (OCV, 3.5 V) to 1.5 V of the mesoporous β-MnO_2 at different rates, 0.03, 0.1, and 0.3, 1 and 2 mA/cm^2. The discharge capacity decreased with increased discharge current density. The capacity of the mesoporous β-MnO_2 electrode at 0.03 mA/cm^2 is 219.4 mA h g^{-1}, while at 0.1, 0.3, 1, and 2 mA/cm^2, it is 189.3, 169.0, 143.6, and 115.2 mA h g^{-1}, respectively. That means at 0.1, 0.3, 1, and 2 mA/cm^2, the capacity retentions are 86.3, 77.0, 65.5, and 52.5%, respectively. Those data of rate capabilities of the mesoporous β-MnO_2 are among the highest values attained for any manganese dioxides.[43−46] This result demonstrates the role of mesoporous structure of β-MnO_2 in facilitating the fast transport and intercalation kinetics of lithium ions: the ordered arrangement guarantees that a rapid charge−discharge process will be complete in a very short time, resulting in a high specific capacity even at a high charge−discharge current.

Figure 8A shows the charge and discharge curves of mesoporous β-MnO_2 at a constant current density of 0.4 mA/cm^2 for the 1st, 2nd, 6th, 10th, 25th, and 50th cycles after the first discharge/charge cycle from the OCV to 1.5 V and then from 1.5 to 4 V, and also the cycle performance and Coulombic efficiency of mesoporous β-MnO_2 can be directly seen in Figure 8B. The first discharge capacity exceeds that of the first charge capacity, and the Coulombic efficiency is about 95%. The irreversible capacity loss observed here is due to the fact that a fraction of the lithium ions inserted during the first discharge become locked within the crystal structure of β-MnO_2 for the lattice stabilization purpose.[47] There is no doubt, however, the charge/discharge efficiency was close to 100% on the subsequent cycling, and the capacity retention was excellent. The mesoporous β-MnO_2 electrode shows a capacity fading of no more than 0.2% per cycle, decreasing from a capacity of 158 mA h g^{-1} in the first to 142 mA h g^{-1} at the 50th cycle. To the best of our knowledge, these data indicate that the cycling reversibility of mesoporous β-MnO_2 is better than those of any reported β-MnO_2 and among the best for any manganese oxides. It is well-known that the lattice parameter *a* increases from 0.440 to 0.454 nm on average with the lithium insertion, while parameter *c* rarely increases,[13] because the *a*-axis is perpendicular to and the *c*-axis is parallel to the direction of the [1 × 1] channels. The lithium ion insertion results in the expansion of the lattice perpendicular to the [1 × 1] channels. The expansion of the lattice resulting from the lithium insertion produces a stress in the particle which will destroy both the nanoarchitecture and the crystalline structure, thus inducing poor performance after a number of charge−discharge cycles. However, the ordered mesoporous structure with the mesoporous channels runs along the *c*-axis and will act as a buffer layer between the β-MnO_2 blocks to alleviate the volume expansion caused by the insertion and extraction of lithium ions, thereby, improving the cycle performance.

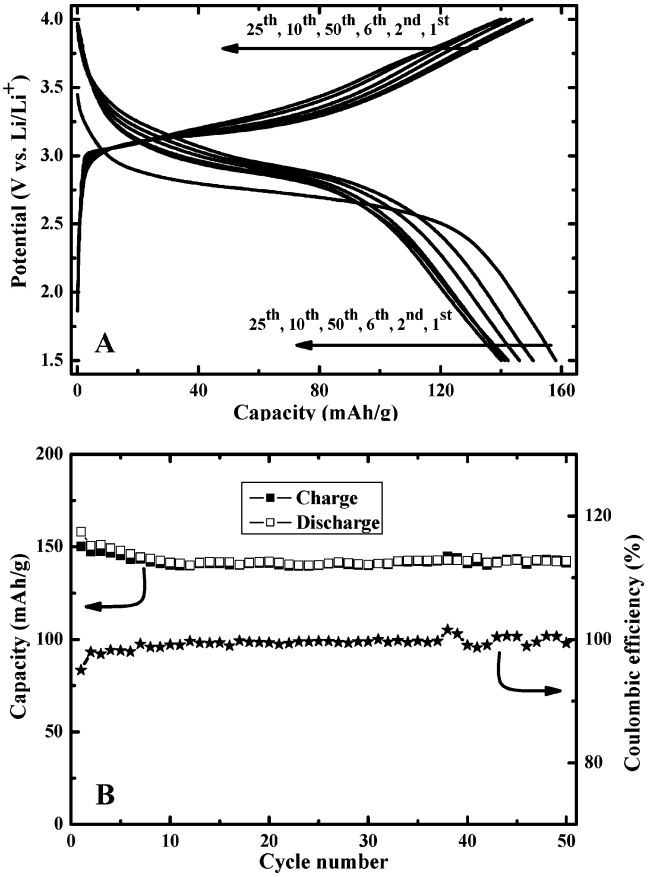

Figure 8. (A) Charge and discharge profiles of mesoporous β-MnO_2 for the 1st, 2nd, 6th, 10th, 25th, and 50th cycles at a current rate of 0.4 mA/cm^2; (B) charge and discharge cycle performance and Coulombic efficiency of mesoporous β-MnO_2 at a current rate of 0.4 mA/cm^2.

Conclusion

The ordered mesoporous β-MnO_2 was successfully synthesized using mesoporous silica KIT-6 as a template. Electrochemical measurements of lithium-ion batteries showed that the as-prepared ordered mesoporous β-MnO_2 electrode exhibits high initial capacity, excellent high rate discharge performance, and supreme cycling reversibility. The designed mesoporous structure can provide larger specific surface area

(43) Xu, J. J.; Jain, G.; Yang, J. S. *Electrochem. Solid-State Lett.* **2002**, *5*, A152.
(44) Kim, J.; Manthiram, A. *Chem. Mater.* **1998**, *10*, 2895.
(45) Kim, J.; Manthiram, A. *Electrochem. Solid-State Lett.* **1999**, *2*, 55.
(46) Kim, J.; Manthiram, A. *Nature* **1997**, *390*, 265.
(47) Sugantha, M.; Ramakrishnan, P. A.; Hermann, A. M.; Warmsingh, C. P.; Ginley, D. S. *Int. J. Hydrogen Energy* **2003**, *28*, 597.

leading to higher current density and a thin pore wall reducing the lithium ion diffusion path. In addition, the mesoporous structure facilitates the fast transport of electrolyte with lithium ion and can also act as a buffer layer to alleviate the volume expansion of the electrode materials during lithiation/delithiation. Therefore, the ordered mesoporous β-MnO_2 can be a promising cathode material in rechargeable lithium-ion batteries. The mesoporous structure described in the present work may also provide a new approach to improve the reaction activity of the materials.

Acknowledgment. This work was partially supported by the National Natural Science Foundation of China (No. 20373014) and the program of New Century Excellent Talents in University of China (2005).

CM061458O